Cyclotron resonance in ultra-low-hole-density narrow *p*-type GaAs/(Al,Ga)As quantum wells

B. E. Cole, J. M. Chamberlain, M. Henini, and T. Cheng
Department of Physics, University of Nottingham, University Park, Nottingham NG7 2RD, United Kingdom

W. Batty
School of Electronic Engineering Science, University of Wales, Bangor, Gwynedd LL57 1UT, United Kingdom

A. Wittlin and J. A. A. J. Perenboom
High Field Magnet Laboratory, University of Nijmegen, Toernooiveld 1, NL-6525 ED Nijmegen, The Netherlands

A. Ardavan, A. Polisski, and J. Singleton
Department of Physics, University of Oxford, Clarendon Laboratory, Oxford, OX1 3PN, United Kingdom
(Received 4 September 1996)

The cyclotron-resonance behavior of a series of *p*-type, low p_s, asymmetrically doped (311)*A* quantum wells has been measured over two orders of magnitude in energy. Landau levels for the structures studied have been calculated for comparison with experiment. The calculations use a rotated Luttinger Hamiltonian and invoke the axial approximation. In the quantum limit and at certain far-infrared energies we observe two resonances widely separated in field. We find at the lowest fields that the samples exhibit a light effective mass. For the narrowest quantum well the cyclotron resonance (CR) broadens and shifts to a slightly lighter mass into the quantum limit, above about 2 T. The CR energy is modeled by inter-Landau-level transitions from the highest level, and a discontinuous evolution to a higher effective mass, observed as the second resonance above 8 T, is explained by crossing of the highest two Landau levels, as modeled in the calculation. The discontinuous evolution to a higher mass is found to shift to lower fields as the well width increases, as suggested from the modeling. For the wider quantum wells the influence of additional anticrossings at intermediate fields, due to the proximity of the second subband, is observed. CR energy for these samples is adequately modeled at energies above and below the region of subband anticrossing. The limitations of the modeling procedure have been discussed and a number of features of the experimental data are explained qualitatively in terms of the expected modifications to the hole Landau-level structure when full Landau-level mixing is incorporated into the modeling. The influence of hole-hole interactions and factors influencing the CR scattering time are also discussed briefly. [S0163-1829(97)08804-8]

I. INTRODUCTION

In GaAs/(Al,Ga)As heterostructures containing two-dimensional (2D) holes, the first ''heavy-hole'' subband (HH1) possesses a small effective mass for motion in the plane close to $k=0$.[1–3] However, the second ''light-hole'' subband (LH1) has a negative mass for motion in the plane close to the origin; thus the first and second subbands approach and anticross at higher k, resulting in highly nonparabolic subband dispersion relationships.[1–3] In heterojunctions, with typical hole densities (p_s) of a few 10^{11} cm^{-2}, the Fermi level is usually to be found in this region of severe nonparabolicity, leading to high, p_s-dependent effective masses and other complex behavior.[4–11] In contrast, in narrow quantum wells (QW) the intersubband separation may be increased, leaving the Fermi energy in a region of the first subband where the light effective mass of the zone center is maintained.[12–14] This ability to tune the effective mass by the choice of Fermi level is particularly felicitous for potential device applications.[13,14] However, quantitative experimental investigation of the band structure of QW structures containing 2D holes has been minimal, largely because of the poor quality of the material available.

The recent optimization of growth on (311) crystal planes has resulted in the fabrication of 2D hole systems (2DHS) of exceptional mobility, with transport scattering times comparable with the best electron samples in the case of heterojunctions.[5,15] This progress has stimulated the investigation of Wigner crystallization[16] and the fractional quantum Hall effect[17] in heterojunctions containing 2DHS. The subband dispersion in zero magnetic field (normal to the plane) has been probed in a qualitative fashion using magnetotunneling spectroscopy and found to be satisfactorily modeled by existing calculations, even for the high-index oriented samples.[18] The Landau-level structure of 2DHS has been studied using the proven technique of cyclotron resonance (CR) in a number of previous works,[4–11,19,20] most of which concentrate on the single heterojunction samples where the highest mobilities are usually achieved. The various notable features of the CR spectra observed include a strongly field- and p_s-dependent CR mass and in some cases the observation of multiple CR transitions, usually in samples of lower mobility and higher carrier density. In addition, the (311)-oriented samples show gaps in the CR spectrum over certain energy ranges[4,6–11,19,20]—an effect due to anticrossing between Landau levels of different subbands. To date the

Landau-level structure of 2D hole systems has been calculated only for the (100),[1–3] (111),[21] and (211) (Ref. 22) directions; in the first case, calculations have been compared with existing CR data for (100) heterojunctions, yielding limited agreement.[1] The importance of hole-hole interactions in modeling the hole excitations in a magnetic field was first alluded to in Ref. 12 and recent experimental data have also demonstrated this effect.[5,15]

In this paper we present results of a study of a range of *p*-type doped quantum wells, comparing comprehensive CR measurements with theoretical models of the hole Landau levels. The modifications to the Landau-level structure due to the extra confinement in narrow QW's has been studied while maintaining low impurity-acceptor scattering by modulation doping the QW on one side only. The samples used are also notable for their extremely low hole density; thus the 2D confinement energy in the narrower wells is essentially due to the (Al,Ga)As barrier rather than due to band bending. Furthermore, the quantum limit is reached by 2 T in most cases, so that filling-factor-dependent effects[4,23] can be excluded at fields above this value. In addition, by reducing the possible transition to only those from the ground Landau level (or lowest two Landau levels, should they cross), comparisons of data and calculations are facilitated. A further advantage in this context is the fact that the anticrossings observed in (311) heterojunctions between Landau levels of different subbands[4,5,10,20] are not expected for the narrow QW's, as the intersubband energy is considerably larger than the cyclotron energy.

The field dependence of the CR can be used as a qualitative probe of the hole subband dispersion relationship; e.g., the transition from the ''light-mass'' character of the HH1 subband at low fields (corresponding to low in-plane *k* vector) to the heavier masses at high fields (corresponding to large in-plane *k* vector) is observable.[12] However, a quantitative comparison requires a full calculation of the Landau-level structure. We have performed such calculations using the (311) Hamiltonian appropriate to our samples, derived from a rotation of the Luttinger Hamiltonian.[24] An approximate potential is used and the Landau levels are derived in the axial approximation. In addition to simplifying the calculations, the axial approximation is useful in identifying the likely strong transitions, since selection rules are well defined in this case. The results of calculations are compared with experimental data. A number of features of the CR spectra are explained in terms of the modifications to the Landau fans expected when the full anisotropy is introduced, resulting in Landau-level mixing.

This paper is organized as follows: the samples and the far-infrared (FIR), millimeter-wave and magnet systems used are described in Sec. II. The experimental data are presented in Sec. III, and the Landau-level calculations are discussed in Sec. IV. The CR data are compared critically with calculations in Sec. V and the origin of the various features observed are discussed schematically in terms of the modification of level crossings, found in the axial approximation, into anticrossings when the Landau level mixing is included. The limits of this model are discussed in Sec. VI and a summary is given in Sec. VII.

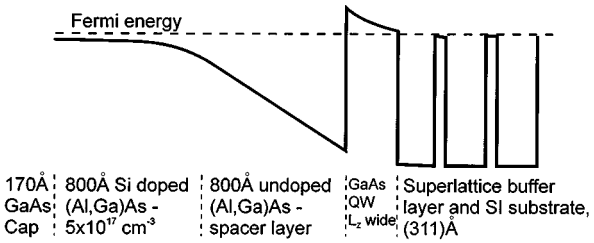

FIG. 1. Valence-band profile of the asymmetrically doped QW structure illustrating the layer sequence.

II. EXPERIMENTAL DETAILS

The samples were prepared using molecular beam epitaxy on (311)*A*-oriented semi-insulating substrates. The layer structure and doping are illustrated in Fig. 1. Silicon is used as a *p*-type dopant for this crystal orientation.[15] The samples were characterized for hole areal density and mobility by low-field Hall effect and magnetoresistance measurements on Hall-bar-type samples; results are given in Table I. Note that mobility is rather anisotropic; values found for Hall bars aligned along the (011) direction, $\mu_\perp$, and the (233) direction, $\mu_\parallel$, differ markedly. This effect is thought to be due to anisotropic scattering by the corrugated (311) GaAs/(Ga,Al)As interface[25] and is enhanced in quantum-well samples compared to heterojunctions. The very high mobilities found in the wide wells are sharply reduced as the well width is decreased. For FIR transmission measurements the samples were lapped to a 2° wedge to avoid interference effects.[26]

The FIR measurements were performed using an optically pumped molecular gas laser and a 20-T Bitter coil. The sample was held at 1.2 K in a pumped ^{4}He bath cryostat. The FIR laser provides a large number of monochromatic FIR laser lines; CR is measured in transmission using a Si bolometer behind the sample while sweeping the magnetic field. The radiation impinging on the sample is unpolarized. A reference bolometer is also used at the laser output to normalize the transmission against fluctuations in laser intensity.

Millimeter-wave measurements were performed in a similar swept-field configuration. A ''millimeter wave vector network analyzer'' (MVNA) (Ref. 27) was used to provide a continuously tunable source and detector of mm-wave radiation from 30–200 GHz. Measurements of the sample transmission were performed at a wide range of frequencies in

TABLE I. Well width, hole areal density, ps, and transport mobility in the (110), $\mu_\perp$, and (233), $\mu_\parallel$, directions for all the samples measured.

Sample ID	L_Z	Characteristics at 2 K		
		p_s	$\mu_\perp$	$\mu_\parallel$
	(Å)	(10^{11} cm^{-2})	(m^2 V^{-1} s^{-1})	
1 (NU1165)	70	0.33	3.1	7.5
2 (NU1166)	85	0.45		6.5
3 (NU944)	150	0.52	66.3	
4 (NU1076)	200	0.6	40	75

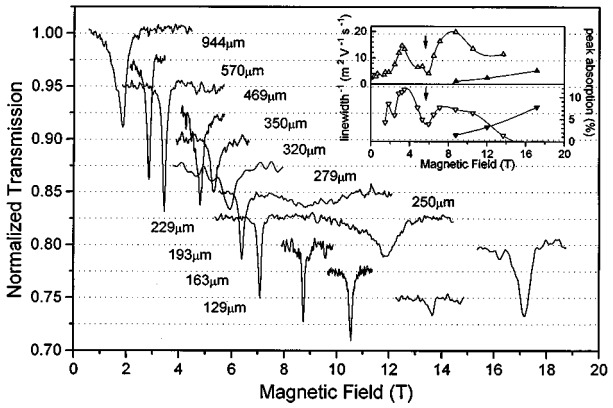

FIG. 2. CR spectra for sample 1 are plotted at a range of FIR laser wavelengths. The inverse linewidths (inset top) and peak resonant absorptions (inset bottom) are plotted for all the wavelengths used for sample 1. Data for the high-energy CR branch are plotted as open triangles and the low-energy CR branch as solid triangles in the inset. The solid lines (inset) are a guide to the eye.

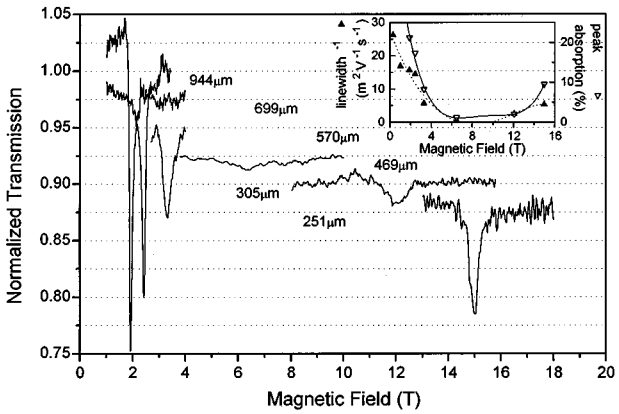

FIG. 3. CR spectra for sample 3 are plotted at a range of FIR laser wavelengths. In the inset are plotted the inverse linewidths (solid triangles) and peak resonant absorptions (open triangles) for sample 3.

this range using an oversized waveguide with the sample cut to fit the waveguide cross section. At mm wavelengths wedging is insufficient to suppress interference effects, as the wavelength in the GaAs substrate is similar to the sample thickness. For such measurements the samples were thinned to 300 μm, but were unwedged, so that Fabry-Pérot-type effects were avoided for wavelengths longer than 4 mm (frequency below 75 GHz). In general, where symmetric absorption line shapes are obtained the resonance position occurs at the transmission minimum,[26] otherwise asymmetric line shapes are fitted by allowing arbitrary mixing of the real and imaginary parts of a Drude-type complex dynamical conductivity. Further measurements were made by placing the sample in a 60-GHz cylindrical resonant cavity; the cavity was then weakly coupled to the MVNA source and detector by narrow apertures and oversized waveguides. The cavity response, on resonance, was measured as a function of magnetic field. In this configuration the sample top surface is separated from the cavity end by a thin sheet of Mylar. The coupling of the sample to the cavity electric field could then be tuned by choice of Mylar thickness in order to obtain cyclotron resonances in the range 10–20 % of the full signal in size. By limiting the sample absorption in this way we ensure a linear response of the cavity and a well controlled electrodynamic environment for the sample. For both transmission and cavity configurations the millimeter radiation is linearly polarized at the sample. The magnetic field was provided by a 17-T superconducting solenoid and the sample was held at 1.4 K in low-pressure exchange gas in contact with a pumped ^{4}He bath.

III. CYCLOTRON RESONANCE RESULTS

Figure 2 shows a compendium of CR spectra, at a number of FIR laser wavelengths, for the sample with a 70-Å well width (sample 1). A striking feature of some short-wavelength data is the observation of *two* resonances (e.g., at 229 μm), widely separated in field. At low fields the CR consists of a single, sharp resonance with linewidths of typically under 0.5 T, although a marked field-dependent CR width and depth is evident; the inverse half-widths (in units of mobility) and peak absorption strengths have been plotted as a function of field in the inset to Fig. 2. Note a minimum in absorption depth (and maximum in linewidth), centered around 5.5 T, is highlighted by an arrow in this inset. The behavior of the 85-Å QW (sample 2) is qualitatively similar, although the minimum CR depth occurs at a lower field, close to 4 T.

CR spectra for the 150-Å QW (sample 3) are shown in Fig. 3 with similar behavior (not shown) found for the 200-Å QW (sample 4). The behavior of the CR in these two wider wells appears to have three characteristic regions. At the longest wavelengths (lowest field) both samples show very sharp resonances ($\Delta B \leqslant 0.3$ T). At higher magnetic field, broad weak CR is observed over an extended range. At the highest fields a sharp CR, consistent with a high sample mobility, is recovered.

CR obtained at millimeter-wave frequencies for samples 3 and 1 is shown in Figs. 4(a) and 4(b) (solid lines), respectively. The resonant fields and linewidths are accurately obtained by fitting the data to a Drude-type expression for the

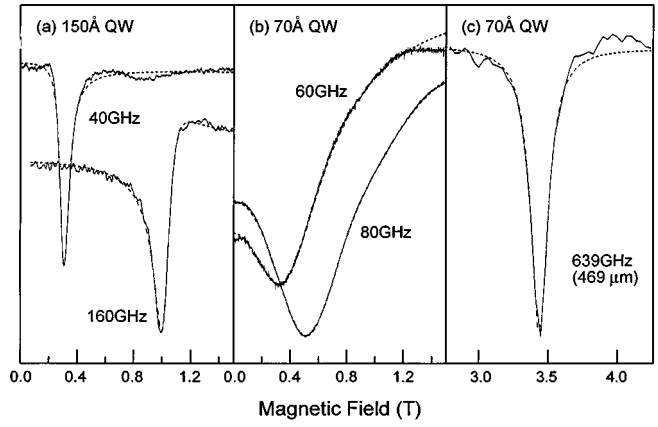

FIG. 4. (a) mm-wave data for sample 3 (solid) obtained in the transmission configuration for 2 wavelengths and fitted line shapes (dotted). (b) mm-wave data for sample 1 (solid) obtained using the resonant cavity configuration and fitted lineshapes (dotted). (c) FIR transmission data for sample 1 at a laser wavelength of 469 μm.

absorbed power and this fitted function is also plotted (dotted lines); the excellent quality of the fits is evident [the discrepancy between the data and fitted function for (a) 40 GHz, at 1 T and also (b) 60 GHz, at 1.5 T is due to a spurious feature at $m^*=1$, which is sample independent and not attributed to the 2DHS]. The asymmetry of the resonances obtained in transmission, as shown in Fig. 4(a), is a consequence of standing waves in the waveguide and in order to fit these data we allow arbitrary mixing between the real and imaginary parts of the dynamical conductivity, $\sigma(\omega)$, where $\sigma=\sigma_+ + \sigma_-$,

$$\sigma_{\pm}(\omega)=\frac{ie^2 p_s}{m^*(\omega\mu\omega_c+i/\tau)}, \quad \omega_c=-eB_{\rm res}/m^*. \qquad (1)$$

τ is the relevant scattering time, $B_{\rm res}$ is the resonant field, and ω is the mm-wave frequency. Measurements using a resonant cavity, as shown in Fig. 4(b), suffer from no such effects and the cavity response is determined solely by the power absorbed in the sample, thus dielectric and interference effects may be discounted. In this case only the real part of $\sigma(\omega)$ is required. For comparison with Fig. 4(b), the FIR transmission data for the same sample (1) at 469 μm (solid line) and the fitted function (dotted line) are plotted in Fig. 4(c) in order to illustrate the dramatic sharpening of the CR found for samples 1 and 2 once the quantum limit is reached. The resonances in Figs. 4(a)–4(c) have all been scaled to a similar size since the magnitude of the resonance depends on the electric-field amplitude at the 2DHG and this differs between measurement configurations.

In the limit of low frequencies the CR mobility $\mu_{\rm CR}$ (inverse linewidth) is a measure of the momentum relaxation time for the center-of-mass motion of the hole system and should tend towards that found in dc transport measurements. Where an anisotropic mobility is found in dc transport measurements the CR may reasonably be expected to measure a scattering time somewhere between $\mu_{\parallel}$ and $\mu_{\perp}$; we find $\mu_{\rm CR}$ to be approximately 60% of the average transport value for both the narrow (1 and 2) and wide (3 and 4) QW samples. Contributions to the scattering from ionized impurities are expected to be small and similar for all the samples. Anisotropic interface roughness scattering is thought to dominate in the (311) p-type structures[25] through the stronger hole confinement at the interface. In the case of the narrow QW's, where scattering at two interfaces may occur and the confinement is even stronger, interface scattering will be very strong, resulting in the large reduction in dc mobility observed in these structures over the wider QW's. As the magnetic field is increased above 2 T, coinciding with $\nu<1$, we observe a pronounced sharpening of the CR for the narrow QW samples (1 and 2) suggesting effective mobilities of up to 200 000 cm^2 V^{-1} s^{-1}, comparable to the narrowest CR observed in the wide, high-mobility QW sample (3 and 4). In contrast the CR for samples 3 and 4 broadens rapidly above 2 T. Maxima in CR linewidth coincident with integer filling factors, such as has been observed in InAs/GaSb and GaAs(Al,Ga)As 2D electron systems,[28] are not observed in our measurements where $\nu>1$.

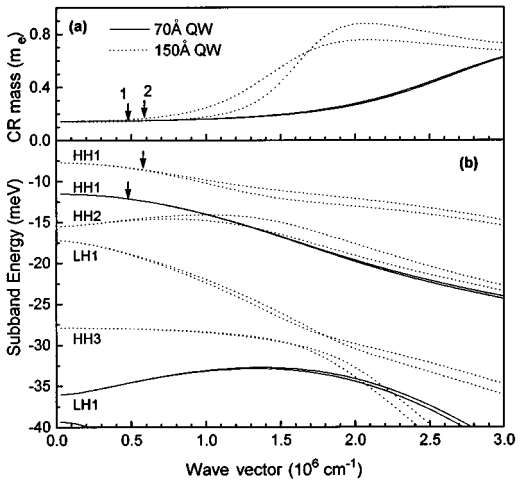

FIG. 5. (a) Semiclassical CR mass, as a function of wave vector, obtained from the zero-field subband dispersion and Eq. (2) (see text) for samples 1 (solid) and 3 (dotted). Arrows indicate the Fermi wave vector for sample 1 (arrow 1) and sample 3 (arrow 2). (b) Zero-field subband dispersions for samples 1 (solid) and 3 (dotted). The subbands are labeled according to their wave-function character at zero wave vector. Energy is measured relative to the valence-band edge.

IV. LANDAU-LEVEL CALCULATIONS

The bulk GaAs valence-band states are accurately described by the four-band ''Luttinger'' Hamiltonian[29] and the heterostructure valence subband dispersion can be derived from the bulk Hamiltonian in the envelope function approximation.[30] The effects of an external magnetic field are readily included by substitution of simple harmonic oscillator raising and lowering operators for the in-plane wave-vector components in the coupled envelope function equations.[1] The Landau levels are obtained from these equations, at finite B, by basis function expansion in terms of the $B=0$ eigenfunctions. Calculations for (100), (111), and (211) orientation heterojunctions, performed previously by other authors[1,2,3,7,21,22] have generally been made in the axial approximation. In one case,[3] however, the inclusion of Landau-level mixing was investigated.

Previous calculations[1–3] involved self-consistent solution of the Poisson and Schrödinger equations. In the present case we avoid having to perform fully self-consistent calculations by approximating the potential due to the hole gas by that obtained from the solution of the Poisson equation for a Fang-Howard wave function in a truncated triangular well. The accuracy of this approximation is enhanced in the narrower, low p_s, QW's where the Coulomb contribution to the confinement energy is small compared with that due to the (Al,Ga)As barriers. In order to calculate the band structure of 2DHS grown on the (311) crystal plane we use a ''rotated'' Luttinger Hamiltonian, applicable to general $[hkk]$-grown structures.[24,31] The single-band, $B=0$ envelope function equations are solved using an accurate shooting method[32] for the particular QW potential shape and then finally Landau levels are calculated in the axial approximation.

The zero-field subband dispersion relationships obtained in this way for the 70-Å and 150-Å QW's are shown in Fig. 5. Also plotted in this figure is the semiclassical CR mass,

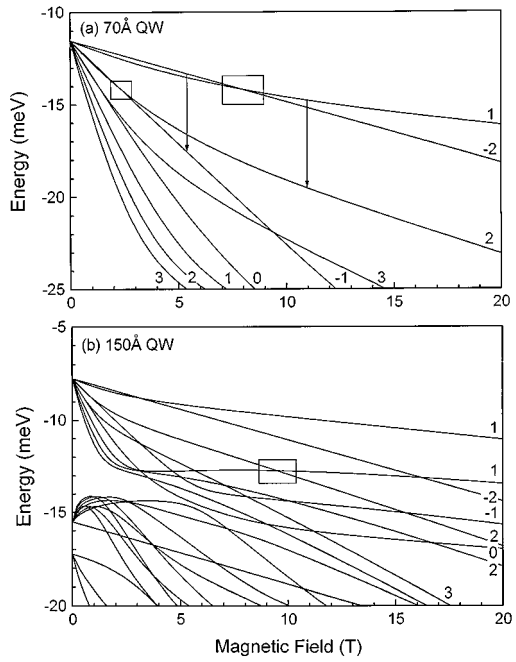

FIG. 6. (a) Landau level fan diagram calculated using the model described in the text for the 70-Å QW (sample 1) is shown. The harmonic oscillator index of each level is marked adjacent to that level and the energy scale is calculated relative to the valence-band edge. The arrows indicate possible CR transitions where all the holes lie in the highest level. Two level crossings have been highlighted by boxes. (b) Landau level fan diagram for the 150-Å QW (sample 3) is shown in a similar manner to (a). Levels originating in the second subband are evident. Additional level crossings occur due to the proximity of second subband such as that highlighted in the box.

$m_{\mathrm{CR}}^{B=0}$, as a function of wave vector, evaluated using

$$m_{\mathrm{CR}}^{B=0}=\frac{\hbar^2}{2\pi}\left.\frac{dA(\varepsilon)}{d\varepsilon}\right|_{\varepsilon}. \tag{2}$$

Here A is the area in k space enclosed by a line of constant energy ϵ. Figures 6(a) and 6(b) display the Landau levels calculated for 70- and 150-Å QW's; analogous results have also been obtained for the 85- and 200-Å QW's studied. In the axial approximation the Landau levels take the form of four series with lowest harmonic oscillator function index, $N=-2$, -1, 0, or 1. Landau levels up to $N=3$ have been plotted and their index numbers are indicated in the figures, adjacent to each level. Note also that a number of level crossings occur. In particular, the $N=1/N=-2$ and the $N=2/N=-1$ crossings [highlighted by boxes in Fig. 6(a)] will be shown to be important in explaining the phenomena observed experimentally for the narrow QW's. These ''intrasubband'' level crossings (i.e., crossings of Landau levels originating from the same subband) are a distinguishing feature of non-(100) Landau levels and are shifted to lower field as the well width increases. In the case of the 150-Å QW, the HH1-HH2 intersubband energy is sufficiently small that intersubband Landau-level crossings (i.e., crossings of Landau levels originating from different subbands) may also occur in the CR energy range studied; such a crossing is highlighted in Fig. 6(b). For all the samples studied the quantum limit is reached by 2.5 T; thus, at magnetic fields above this value inter-Landau-level transitions may only occur from the highest level. In the axial approximation, CR transitions have the selection rule $\Delta N=\pm 1$. The observed CR may therefore be associated with the transitions indicated by the arrows in Fig. 6(a).

V. COMPARISON OF MODELING AND EXPERIMENT

The experimental CR energies and the calculated $N=1\rightarrow N=2$ and the $N=-2\rightarrow N=-1$ transition energies are plotted against field for the 70-, 85-, 150-, and 200-Å QW's in Figs. 7(a)–7(d), respectively. In Figs. 8(a)–8(d) the same data are plotted in the form of CR mass, $m^*=eB/\omega_c$, as a function of field. In the case of the 70- and 85-Å QW's the observed CR energies are in reasonable agreement with the calculated transitions between the levels indicated. From 2 to 8 T the $N=-2\rightarrow N=-1$ transition energy increases almost linearly with magnetic field, resulting in a constant mass ($\sim 0.16m_e$), which is in good agreement with the experimental data. As has been mentioned above, such light in-plane masses are characteristic of the HH1 subband close to the zone center.[12] Below about 2–2.5 T, transitions between higher Landau levels must be considered; however, these are expected to show a similar light mass character since the highest subband tends towards parabolic at the zone center. A small increase in CR mass may be expected as the field falls below the quantum limit and the $n=1\rightarrow n=2$ transition marked in Figs. 7 and 8 become possible once more. Further fluctuations in CR mass as the filling factor increases, as observed previously in p-type heterojunctions of higher p_s,[4] should decrease in amplitude toward the zero-field limit and the CR mass is expected to converge with the zero-field subband mass at the Fermi energy in this limit.[1] In Figs. 8(a)–8(c) the CR mass appears to have a zero-field limit at $(0.17–0.18)m_e$, somewhat higher than $0.15m_e$ expected from the zero-field subband calculations (shown in Fig. 5). Possible reasons for this apparent mass enhancement at low fields are discussed briefly in Sec. VI.

A changeover in oscillator strength from a high-energy to a low-energy branch at fields above 8 T observed in the experimental data for sample 1 is explained by the crossing of the two highest Landau levels, $N=-2$ and $N=1$. The lower-energy branch is in good agreement with the $N=1\rightarrow N=2$ energy found in the calculations. The field range over which the transition between the two branches occurs moves to lower field as the lateral confinement is reduced; for the 200-Å QW the mass increases sharply over the range 2–8 T in a manner similar to that found in CR measurements of heterojunctions containing 2D holes,[4,5] which form the limiting case of an infinitely wide asymmetric QW.

The field positions of the various calculated level crossings [highlighted in Figs. 6(a) and 6(b)] may now be compared with the experimental CR spectra in which two resonances are observed. In making such a comparison, the consequences of the approximations involved in the modeling must be emphasized. It has been shown[31] that in (111)-oriented samples, admixture of levels occurs when $\Delta N=\pm 3$. Similarly, for (100) samples, $\Delta N=\pm 4$ are strongly hybridized. For the (311), low-symmetry orientation, mixing be-

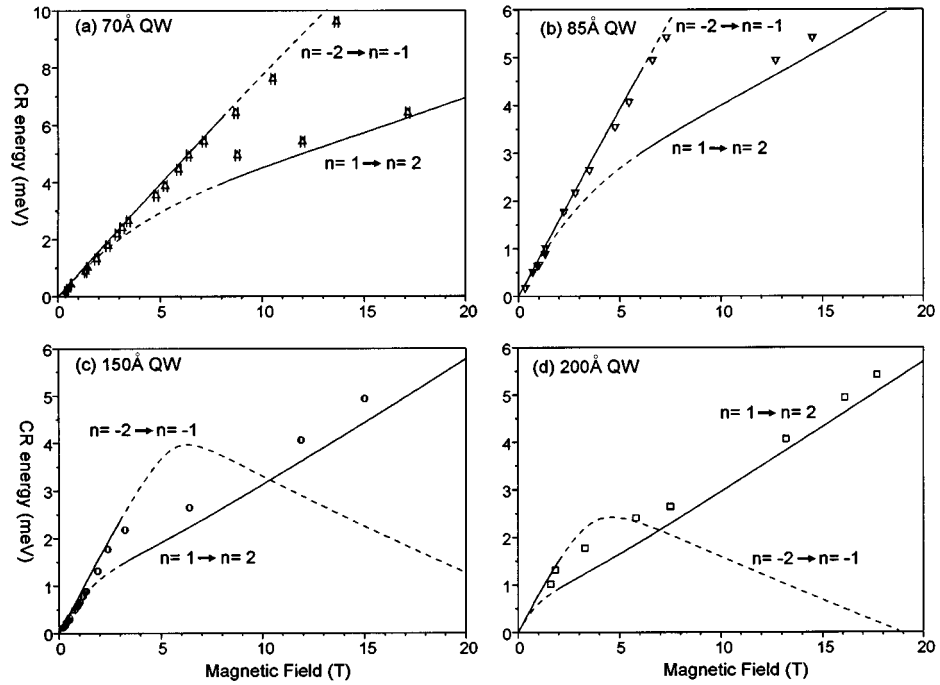

FIG. 7. The measured CR energies are plotted for each field value. The transition energy for the two transitions $n=-2\rightarrow n=-1$ and $n=1\rightarrow n=2$, as calculated in the model described in the text, are plotted for comparison. Where the transition is forbidden (at zero temperature) through either an empty initial state or a completely filled final state, the transition energy is plotted as a dashed line. (a)–(d) show results for samples 1–4, respectively.

tween levels of both $\Delta N=\pm 3$ and $\Delta N=\pm 4$ is possible; thus the ground-state crossing shown in the axial approximation will become an anticrossing once full level mixing is introduced. Where the top Landau level has mixed character, transitions to both the $N=2$ and $N=-1$ levels (as labeled in the axial scheme) are possible from this state. At low fields all the oscillator strength will lie in a transition of character $N=-2\rightarrow N=-1$, however, as the field evolves through the region where mixing of the top two Landau levels occurs the oscillator strength will transfer smoothly to a transition of character $N=1\rightarrow N=2$ found at high fields. This changeover will occur over an extended field range centered around

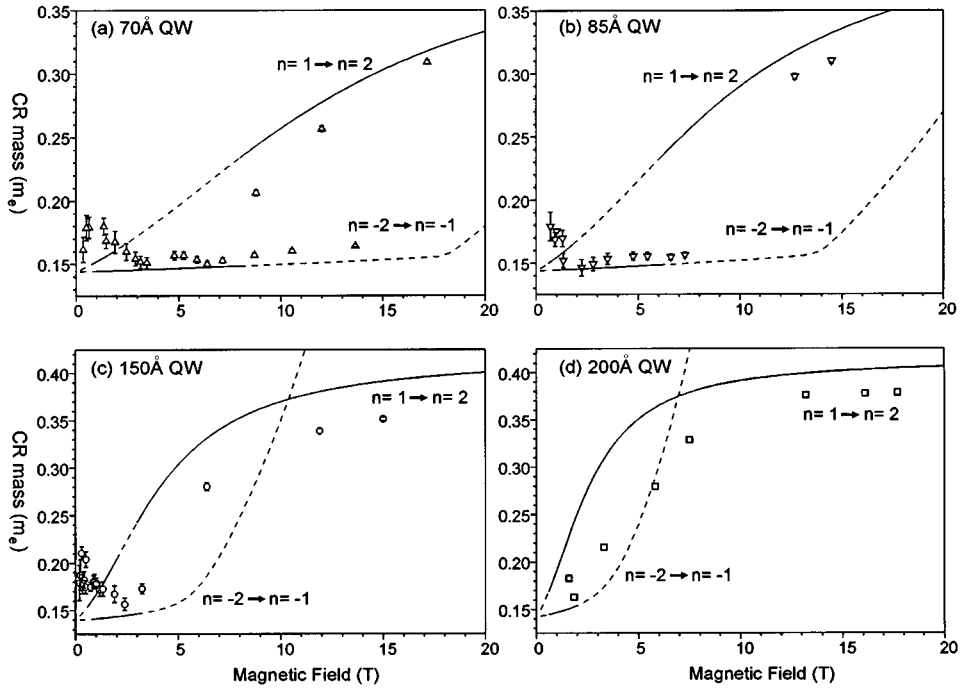

FIG. 8. The same data as plotted in Fig. 7 are shown in the form of CR mass $(=eB/\omega_c)$ as a function of magnetic field. (a)–(d) show results for samples 1–4, respectively.

a field corresponding to equal admixture of the $N=-2$ and $N=1$ states in the initial hole level. Even in the absence of level mixing, however, an extended changeover region is expected; at 1.4 K, the temperature at which the present experiments are performed, the two highest Landau levels have energy separation (in the axial scheme) less than kT ($=0.12$ meV) over a 2-T range around the crossing field. Thus significant thermal population of the two highest Landau levels will occur over a similar field range, leading to the simultaneous observation of two CR in the experimental spectra, and a gradual shift in oscillator strength from one CR to the other. Thus we are not able to clearly distinguish the extent of level mixing from our measurements at this temperature. For comparison with the calculation, an estimation of the field at which the two CR branches have equal absorption strengths is used as a value of the ground-state crossing field. A value of 12 T is thus estimated for the 70-Å QW whereas the calculations suggest a field of 8 T.

The crossing between third ($N=-1$) and fourth ($N=2$) levels in the axial model may explain the minima in peak absorption strength observed in the 70- and 85-Å QW's at 5.5 and 4 T, respectively (see inset to Fig. 2). In the fully mixed scheme the resulting anticrossing (between levels forming the final state of a CR transition) will result in the division of oscillator strength between transitions to the anticrossing levels. Thus the peak absorption strength is reduced. We do not resolve the two possible transitions but do observe a broadening of the CR at a corresponding field (minima in inverse linewidth marked in inset to Fig. 2). As in the case of the ground-state anticrossing, the measured field positions of these two CR oscillator strength minima (5.5 and 4 T) are somewhat higher than those suggested from the calculations (3.5 and 2 T for the 70- and 85-Å QW's respectively).

We point out here that the field of equal admixture of two coupled levels will lie at the crossing field of the unmixed case only to first order in perturbation; when full level mixing is introduced this will not generally be the case. Thus the experimental evidence suggesting level anticrossings at fields above that suggested from the crossing position of unmixed levels is consistent with the nature of the axial approximation.

In the case of the two wider QW's, the ground-state crossings are predicted to be at 3.2 and 2 T for the 150- and 200-Å QW samples, respectively. Below these fields, the light character effective mass expected in the low-field limit is apparent. Note that the CR mass of the 150-Å QW sample has an apparent minimum at 2.5 T where the quantum limit is reached; at fields below this the $N=1\rightarrow N=2$ and other higher transition contribute to the overall mass, however, as with the 70- and 85-Å QW samples, there is no evidence that the CR mass converges with that calculated from the zero-field subband in the low-field limit. Experimentally, the two resonances expected where the bottom two Landau levels cross are not observed although the CR becomes very broad and weak at fields above these values. Above 12 T, sharp resonances are once more obtained with CR masses similar to the calculated $N=1\rightarrow N=2$ transition. Over the field ranges where very weak broad CR was obtained a number of factors may be influencing the results. The large down-turn in energy of the $N=-2\rightarrow N=-1$ transition is a result of anticrossing of the $N=-1$ level with levels associated with the next subband. It is reasonable to expect the character of the $N=-1$ level to change somewhat over this region, reducing the strength of CR transitions to this state. Furthermore, there is strong experimental evidence that the crossing of Landau levels from different subbands highlighted by the box in Fig. 6(b) is an anticrossing.[4,5] Such an anticrossing results in a gap in the CR energy as a function of field such that when this region is probed in the ''constant energy-swept field'' arrangement used in the present experiments, weak or no CR is observed; this is analogous to CR in the electron system in a tilted magnetic field, where the in-plane component of the field mixes Landau levels of different subbands.[23,33] In our hole systems the level mixing is intrinsic to the (311) Hamiltonian and requires no in-plane field. The absence of any resonance at 2.18 meV in the 200-Å QW, despite a very low noise level, may be attributed to this phenomenon. The energy at which this anticrossing occurs in (311) heterojunctions was found[5] to scale with hole density and, for a heterojunction of similar density to the 200-Å QW measured here, the effect occurred at a slightly lower energy. This fact is consistent with the weak contribution that the QW confinement makes to the intersubband separation in this sample.

VI. DISCUSSION

The calculations described in the present work appear to describe the CR energy for the 70- and 85-Å quantum wells adequately in the quantum limit. The axial approximation is known to work reasonably well for (111) and (100) heterostructures[31] (i.e., structures in which the in-plane anisotropy vanishes completely at the zone center). Although zero-field subband calculations show some anisotropy in the (311) QW's the CR is insensitive to this, being a form of in-plane average around the Fermi surface [see Eq. (1)]. A useful aspect of the axial approximation is the well-defined labeling of levels by harmonic oscillator number and the selection rule $\Delta N=\pm 1$ for CR transitions in this scheme. Transitions allowed in the axial approximation may be expected to dominate when full mixing is introduced.[1,3,31] The axial approximation calculations also provide an explanation for both the discontinuous crossover from low to high CR mass and the field dependence of the CR oscillator strength and linewidth in terms of crossing of various Landau levels. However, the field position of these phenomena is not well predicted by the axial calculation; the predicted crossings occur at somewhat lower fields than suggested by experiment. To account for this more fully the Landau-level mixing must be taken into account; no calculations yet exist for (311) samples including full level mixing. Although, to first order, the field of equal admixture of two unmixed states occurs at the crossing field, higher-order effects may not be ignored. We note that exact calculations for a (111) heterojunction in which states of $\Delta N=\pm 3$ mix show the two (anti)crossings mentioned above shifted to higher fields by a significant amount in comparison with an axial calculation.[31]

In applying our modeling procedure to the wider QW structures the observed trends are borne out. However, at intermediate fields (where the cyclotron energy is comparable to the intersubband-Landau-level energy) the axial ap-

proximation proves inadequate; the number of level crossings that may mix in an exact calculation make a quantitative interpretation in the axial scheme difficult. Furthermore, the exact shape of the potential well is sensitive to the level and nature of the background doping. For (311) samples where Si incorporates as an acceptor the background doping will be *p* type overall although the net acceptor concentration is not well known. The approximate potential used is expected to be least accurate when modeling an accumulation layer; for 200- and 150-Å QW's the well confinement adds to the subband energy only slightly so any error in the approximate potential will be more pronounced than for the narrower QW's.

The influence of the Coulomb interaction between holes may also contribute to the difference between the model predictions and the experimental data. This interaction has been shown[4,19] to couple cyclotron motion of holes undergoing transitions of different frequency to a single frequency hybrid resonance. In the situation where the first and second Landau levels cross and an equal number of holes reside in each level, the Coulomb interaction can, in principle, couple the two transitions of different energy to a single-energy hybrid resonance. A model describing the analogous effect in 2D electron systems has been derived by Cooper and Chalker;[34] it was found that the criterion for observation of strong Coulombic coupling was that a dimensionless coupling constant defined in Ref. 34 should be at least 0.05. In the quantum limit, the strength of the Coulomb coupling scales with magnetic length and hole density;[34] for the case of the low density, narrow QW's (where the crossover from light to heavy CR mass occurs far into the quantum limit) the Coulombic interactions are likely to be small as the dimensionless coupling constant is ~ 0.01 at the crossover region for the 70-Å QW. Both CR branches for this sample appear to deviate from the calculated transition energies as the oscillator strength decreases; this may perhaps be a manifestation of weak Coulombic coupling. As the crossover region moves to lower field, the Coulomb coupling strength increases and a single resonance, as predicted by Ref. 34, is indeed observed throughout this region (see also the discussion in Refs. 4 and 19).

Out of the quantum limit interpretation of the CR in terms of single-particle Landau-level transitions is less useful. It has become evident that a full interpretation of CR in 2D electron systems, despite a simple bare electron band structure, is complicated due to the self-consistent interaction of the electrons with one another, the lattice and disorder. Thus we do not attempt a complete interpretation of CR in the more complex 2DHS in the region of $\nu \geq 1$ but limit ourselves to the comments below. Thermal population of higher levels becomes significant, increasing the number of levels involved in CR transitions dramatically and the strong coupling of CR transitions through hole-hole scattering results in a resonance that is a hybrid of the many possible single-particle modes.[19] At the lowest CR frequencies the conditions for semiclassical CR are fulfilled, namely, that $\eta\omega \ll E_F$ and $kT \ll E_F$, where E_F is the Fermi energy. The apparent discrepancy between the zero-field intercepts of the measured CR masses with the calculated subband CR mass is surprising given the good agreement obtained in the quantum limit. The approximations of the model, in terms of QW potential shape and axial symmetry, are least severe for the narrowest QW's and at the smallest cyclotron energies. We note the CR broadening to lower fields occurs simultaneously with the shift up in mass; similar behavior has been found in 2D electron systems in both Si inversion layers[35] and GaAs/(Al,Ga)As (311)*B* heterostructures[36] and was interpreted as being due to a disorder-pinned charge-density wave (CDW) state in the first case and to coupling of the CR to the magnetoplasmon modes through disorder in the second. The CDW state implicated in Ref. 35 is suggested to form in the quantum limit, shifting the measured CR mass to below the bare band mass. Conversely the magnetoplasmon coupling suggested in Ref. 36 tends to enhance the CR mass over the bare value where $\nu > 1$; this explanation would appear to fit our data more closely. A number of other factors may contribute to the sharpening of the CR at $\nu < 1$, independent of the shift in CR mass, such as the range of the scattering potential and screening effects. In the first case a disorder potential of range greater than the cyclotron radius *R* does not contribute significantly to the CR linewidth,[37] hence a narrowing of the CR occurs where *R* falls below the range of the interface inhomogeneity. Secondly, screening of a long-range potential (whose effectiveness increases with the density of states at the Fermi level) will be greater in the quantum limit where the density of states at the Fermi level increases with field.[38] In samples 3 and 4 the CR linewidth is dominated by band-structure effects such as severe nonparabolicity and intersubband Landau level anticrossings at fields above 2 T, due to the proximity of the second subband, thus a sharpening of the CR in the manner observed for the narrow QW samples would be masked. In addition, impurity scattering may not be completely insignificant in the wide QW's leading to different linewidth behavior in the wide QW's.

VII. CONCLUSIONS

In conclusion, we have measured the cyclotron resonance behavior of a series of *p*-type, low p_s, asymmetrically doped (311) QW's over two orders of magnitude in energy. Landau levels for the structures studied have been calculated for comparison with experiment. The calculations use a rotated Luttinger Hamiltonian and invoke the axial approximation.

We find at the lowest fields that the samples exhibit a light effective mass, typically $m^* = 0.17 m_e$, characteristic of the HH1 subband zone center although this value is slightly above the semiclassical CR mass of $m^* = 0.14 m_e$ found from the zero-field subband dispersion. Above about 2 T, the samples are fully quantized by the magnetic field and the CR energy is modeled by inter-Landau-level transitions from the highest level. In this field range the CR mass for the 70- and 85-Å QW's is found to be roughly constant with energy in accordance with the $N = -2 \rightarrow N = -1$ transition calculated in the axial scheme and a mass of $m^* = 0.15 m_e$ is obtained. The oscillator strength of this transition is lost at high magnetic fields while that of a lower-energy CR branch is seen to develop. This is explained by crossing of the two lowest ($N = -2$ and $N = 1$) Landau levels at an intermediate field; above this crossing field the ground state assumes a $N = 1$ character and the CR energy is then satisfactorily modeled by the $N = 1 \rightarrow N = 2$ transition. In addition we find minima in

the oscillator strength as a function of field that may be explained by anticrossing of the third and fourth Landau levels; these levels ($N=2$ and $N=-1$) are predicted to cross in the axial approximation calculations but are expected to mix in the exact calculation. Experimentally, the field range over which the CR mass evolves form a low to high value shifts to lower fields for wider QW widths; this trend is also reproduced by the modeling. In contrast, two distinct CR branches are *not* observed in the case of the two wider QW's; weak, broad CR is found at energies intermediate to the two branches suggested by the calculated $N=-2\rightarrow N=-1$ and $N=1\rightarrow N=2$ transitions. Additional anticrossings, at these intermediate fields, due to the proximity of the second subband complicate the CR spectrum of the 150- and 200-Å samples, however, the CR energy is adequately modeled at energies above and below this region.

The limitations of the modeling procedure have been discussed and a number of features of the experimental data are explained qualitatively in terms of the expected modifications to the hole Landau-level structure when full Landau-level mixing is incorporated into the modeling. The influence of hole-hole interactions and factors influencing the CR scattering time have also been discussed briefly.

ACKNOWLEDGMENTS

This work was carried out as part of Engineering and Physical Sciences Research Council (EPSRC) research programmes at Nottingham and Oxford. B.E.C. acknowledges EPSRC for financial support. Work at KU Nijmegen is supported by the Commission of the European Communities under the Large Installation Programme and the Stichting voor Fundameteel Onderzoek der Materie (FOM). Phillippe Goy, Mark Witney and Dennis Rawlings have provided invaluable technical assistance with the construction of microwave equipment.

[1] U. Ekenberg and M. Altarelli, Phys. Rev. B **32**, 3712 (1985).
[2] D. A. Broido and L. J. Sham, Phys. Rev. B **31**, 888 (1985).
[3] E. Bangert and G. Landwehr, Surf. Sci. **170**, 593 (1986).
[4] S. O. Hill, B. E. Cole, J. Singleton, J. M. Chamberlain, P. J. Rodgers, T. J. B. M. Janssen, P. A. Pattenden, B. L. Gallagher, G. Hill, and M. Henini, Physica B **211**, 440 (1995).
[5] S. J. Hawksworth, S. Hill, T. J. B. M. Janssen, J. M. Chamberlain, J. Singleton, U. Ekenberg, G. M. Summers, G. A. Davies, R. J. Nicholas, E. C. Valadares, M. Henini, and J. A. A. J. Perenboom, Semicond. Sci. Technol. **8**, 1465 (1993).
[6] H. L. Störmer, Z. Schlesinger, A. Chang, D. C. Tsui, A. C. Gossard, and W. Wiegmann, Phys. Rev. Lett. **51**, 126 (1983).
[7] Z. Schlesinger, S. J. Allen, Y. Yafet, A. C. Gossard, and W. Wiegmann, Phys. Rev. B **32**, 5231 (1985).
[8] W. Erhardt, W. Staguhn, P. Byszewski, M. von Ortenberg, G. Landwehr, G. Weimann, L. van Bockstal, P. Janssen, F. Herlach, and J. Witters, Surf. Sci. **170**, 581 (1986).
[9] Y. Iwasa, N. Miura, S. Tarucha, H. Okamoto, and T. Ando, Surf. Sci. **170**, 587 (1986).
[10] Z. Schlesinger and W. I. Wang, Phys. Rev. B **33**, 8867 (1986).
[11] G. A. Davies, Ph.D. thesis, University of Cambridge (1991).
[12] A. S. Plaut, J. Singleton, R. J. Nicholas, R. T. Harley, S. R. Andrews, and C. T. B. Foxon, Phys. Rev. B **38**, 1323 (1988).
[13] E. P. O'Reilly, Semicond. Sci. Technol. **4**, 121 (1989).
[14] D. Lancefield, W. Batty, C. G. Crookes, E. P. O'Reilly, A. R. Adams, K. P. Homewood, G. Sundaram, R. J. Nicholas, M. Emeny, and C. R. Whitehouse, Surf. Sci. **229**, 122 (1990).
[15] M. Henini, P. J. Rodgers, P. A. Crump, and B. L. Gallagher, Appl. Phys. Lett. **65**, 2054 (1994).
[16] P. J. Rodgers, C. J. G. M. Langerak, B. L. Gallagher, R. J. Barraclough, M. Henini, T. J. Foster, G. Hill, S. A. J. Wiegers, and J. A. A. J. Perenboom, Physica B **184**, 195 (1993).
[17] E. E. Mendez, Surf. Sci. **170**, 561 (1986).
[18] R. K. Hayden, L. Eaves, M. Henini, E. C. Valadares, O. Kühn, D. K. Maudes, J. C. Portal, T. Takamasu, N. Miura, and U. Ekenburg, Semicond. Sci. Technol. **9**, 298 (1994).
[19] B. E. Cole, W. Batty, A. Ardavan, S. O. Hill, A. Polisski, X. Li, L. van Bockstal, J. Singleton, J. M. Chamberlain, M. Henini, and T. Cheng (unpublished).
[20] K. Hirakawa, Y. Zhao, M. B. Santos, M. Shayegan, and D. C. Tsui, Phys. Rev. B **47**, 4076 (1993).
[21] D. J. Barnes, R. J. Nicholas, R. J. Warburton, N. J. Mason, P. J. Walker, and N. Miura, Phys. Rev. B **49**, 10 474 (1994).
[22] C. A. Hoffman, J. R. Meyer, R. J. Wagner, F. J. Bartoli, X. Chu, J. P. Faurie, L. R. Ram-Mohan, and H. Xie, J. Vac. Sci. Technol. A **8**, 1200 (1990).
[23] R. J. Nicholas, M. A. Hopkins, D. J. Barnes, M. A. Brummell, H. Sigg, D. Heitmann, K. Ensslin, J. J. Harris, C. T. Foxon, and G. Weimann, Phys. Rev. B **39**, 10 955 (1989).
[24] B. E. Cole, W. Batty, Y. Imanaka, Y. Shimamoto, J. Singleton, J. M. Chamberlain, N. Miura, M. Henini, and T. Cheng, J. Phys. Condens. Matter **7**, L675 (1995).
[25] M. Henini, P. J. Rodgers, P. A. Crump, B. L. Gallagher, and G. Hill, Appl. Phys. Lett. **65**, 2054 (1994).
[26] M. von Ortenberg, Solid State Commun. **17**, 1335 (1975).
[27] P. Goy, French Patent No. CNRS-ENS, 1989; P. Goy, U.S. Patent No. 5 119 035 (2 June 1992).
[28] D. Heitmann, M. Ziesmann, and L. L. Chang, Phys. Rev. B **34**, 7463 (1986).
[29] J. M. Luttinger, Phys. Rev. **102**, 1030 (1956).
[30] G. Bastard, *Wave Mechanics Applied to Semiconductor Heterostructures* (Les Editions de Physique, Les Ulis, 1988).
[31] W. Batty, B. E. Cole, J. M. Chambelain, and J. Singleton, Proceedings of the 23 at International Conference on the Physics of Semiconductors (World Scientific, Singapore, in press).
[32] S. P. Wilson and D. W. E. Allsopp, Superlattices Microstruct. **11**, 363 (1992).
[33] G. L. J. A. Rikken, H. Sigg, C. J. G. M. Langerak, H. W. Myron, J. A. A. J. Perenboom, and G. Weimann, Phys. Rev. B **34**, 5590 (1986).
[34] N. R. Cooper and J. T. Chalker, Phys. Rev. Lett. **72**, 2057 (1994).
[35] B. A. Wilson, S. J. Allen, Jr., and D. C. Tsui, Phys. Rev. B **24**, 5887 (1981).
[36] Z. Schlesinger, W. I. Wang, and A. H. MacDonald, Phys. Rev. Lett. **58**, 73 (1987).
[37] T. Ando and Y. Murayama, J. Phys. Soc. Jpn. **54**, 1519 (1985).
[38] R. Lassnig and E. Gornik, Solid State Commun. **47**, 959 (1983).